



## Research paper

Design and biological evaluation of novel triaryl pyrazoline derivatives with dioxane moiety for selective BRAF<sup>V600E</sup> inhibition

Hong-Lin Li<sup>a,1</sup>, Mi-Mi Su<sup>a,1</sup>, Yun-Jie Xu<sup>a</sup>, Chen Xu<sup>a,\*\*\*</sup>, Yu-Shun Yang<sup>a,b,\*\*</sup>, Hai-Liang Zhu<sup>a,b,\*</sup>

<sup>a</sup> State Key Laboratory of Pharmaceutical Biotechnology, Nanjing University, Nanjing, 210023, China

<sup>b</sup> Institute of Chemistry and BioMedical Sciences, School of Chemistry and Chemical Engineering, Nanjing University, Nanjing, 210023, China

## ARTICLE INFO

## Article history:

Received 28 May 2018

Received in revised form

14 June 2018

Accepted 16 June 2018

Available online 19 June 2018

## Keywords:

Triaryl pyrazoline

Dioxane

Antitumor

Apoptosis induction

BRAF<sup>V600E</sup>

Selectivity

## ABSTRACT

A series of novel selective BRAF<sup>V600E</sup> inhibitory agents (Compound **1–16**) 5-(2,3-dihydrobenzo[*b*][1,4]dioxane-6-yl)-*N*,3-diaryl-4,5-dihydro-1*H*-pyrazole-1-carbothioamides have been designed and synthesized. Their anti-proliferation and BRAF inhibitory activities were evaluated. Though **15**, **4** and **12** all displayed comparable activity with the positive control Vemurafenib, only **12** indicated fine selectivity on BRAF<sup>V600E</sup> (IC<sub>50</sub> = 0.06 μM for BRAF<sup>V600E</sup>; GI<sub>50</sub> = 0.52 μM for A375) over BRAF<sup>WT</sup> at both kinase and cell levels. This result satisfied the designing concept of improving activity and introducing selectivity. Flow cytometry analysis and western blot convinced the apoptosis induction and kinase inhibitory activity. Docking simulation inferred the differences in binding patterns of BRAF<sup>V600E</sup> and BRAF<sup>WT</sup>, pointing out that the future orientation might be seeking for outer space binding of BRAF<sup>V600E</sup> and avoiding interactions with HIS573 of BRAF<sup>WT</sup>. These results brought potent BRAF inhibitors one step further to selective agents, enhancing the potential for safe medication.

© 2018 Elsevier Masson SAS. All rights reserved.

## 1. Introduction

Risking the health of people worldwide, cancer pushed thousands of researchers to develop novel agents and therapeutic methods continuously despite the achievements made in medicinal chemistry [1].

Classical MAPK pathway participates in vital cell procedures such as proliferation and survival [2,3], and has been convinced hyper-activated in up to 30% of human cancers [4–8]. All through its RAS-RAF-MEK-ERK cascade, RAF involved activating mutations have been most reported. In these reports, RAF showed innegligible high relativity (50–70%) to melanoma [9], followed by thyroid cancer [10–12] and ovarian cancer [13–15]. Inhibiting RAF was believed to be an effective solution for treating cancer [16,17]. BRAF

was the most frequently mutated RAF kinases isoform, and noticeably, near 90% of its activating mutations in cancers are substitution of VAL for GLU (V600E, formally defined as V599E) [18,19]. Such mutations resulted in a 500-fold MEK phosphorylation basal rate increase over wild-type BRAF (BRAF<sup>WT</sup>) [20] and consequently stimulation of tumor growth and vascular endothelial growth factor secretion [21,22]. Since BRAF was essential for normal cell procedure [23,24] whereas BRAF<sup>V600E</sup> was proved momentous for tumorigenesis, inhibiting undesirable BRAF mutations without interfering BRAF<sup>WT</sup> has become potential hotspot for potent inhibition and safe medication [25–27].

At present, Vemurafenib was still the top FDA approval BRAF inhibitor with explicit design and mechanism [28]. It was the first agent designed using fragment-based drug discovery (FBDD). Unlike Dabrafenib or Encorafenib which were usually used in combination with MEK inhibitors, Vemurafenib was specific for BRAF<sup>V600E</sup> with known binding pattern (Fig. 1). Seeking alternative backbones to avoid the 7-azaindole moiety with possible side effect led to modification of triarylimidazole derivative SB-590885 [29,30]. Considering the binding pattern of Vemurafenib into BRAF<sup>V600E</sup> (PDB code: 3OG7) and consulting that of SB-590885 (PDB code: 2FB8), we should retain interactions with key residues including PHE583, LYS483 and TRP531. In our previous work, we

\* Corresponding author. State Key Laboratory of Pharmaceutical Biotechnology, Nanjing University, Nanjing, 210023, China.

\*\* Corresponding author. State Key Laboratory of Pharmaceutical Biotechnology, Nanjing University, Nanjing, 210023, China.

\*\*\* Corresponding author.

E-mail addresses: [xuchn@nju.edu.cn](mailto:xuchn@nju.edu.cn) (C. Xu), [ys\\_yang@nju.edu.cn](mailto:ys_yang@nju.edu.cn) (Y.-S. Yang), [zhuhl@nju.edu.cn](mailto:zhuhl@nju.edu.cn) (H.-L. Zhu).

<sup>1</sup> Both authors contributed equally to the work.

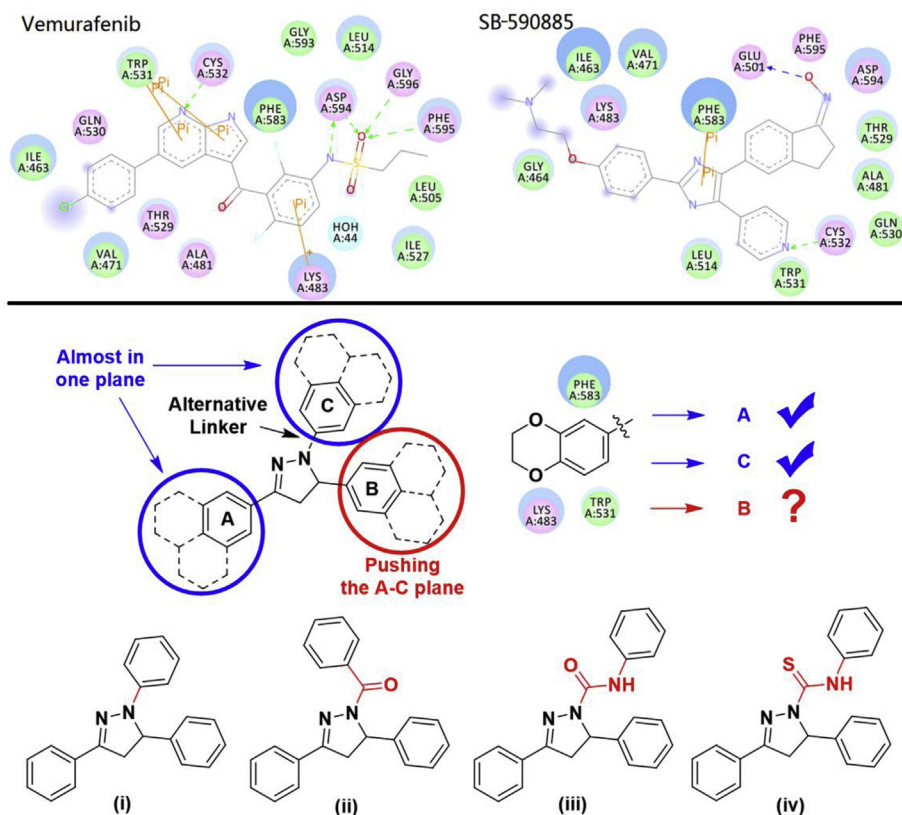


Fig. 1. Binding patterns of Vemurafenib and SB-590885 inspired our design concept of rotating dioxane-containing group to Ring B and choosing suitable linker.

built and discussed the ABC-ring system of 1,3,5-triaryl pyrazoline series BRAF inhibitors as shown in Fig. 1 [31–33]. Ring A and C were almost in one plane while Ring B indicated an angle with this plane. The selected 1,4-benzodioxane group was introduced because of its merits on improving druggability (such as LogP and PSA) and binding mode (enhancing interactions with LYS483 [32], TRP531 and PHE583 [33]). Previous also pointed out audacious modification orientation of stretching the backbone to outer space or totally reversing it [33], therefore we conducted cautious rotation of ABC rings with fine regulation in this work. In consideration of consistency and previous brought merits, we retained 1,4-benzodioxane group and fixed it at Ring B. The ABC-ring backbone distinguished this series from other dioxane-containing agents and avoided off-target effect [34,35]. As for the alternative linker, we recognized that when we fixed Ring B as 1,4-benzodioxane, it started to affect the steric conformation of A-C plane. Ring A was basically fixed within the plane due to the conjugated double bond in pyrazoline. However, Ring C could still be allowed to rotate finitely. An ideal situation for carrying out rational design demanded that Ring C should be better restricted within the same plane of Ring A. Therefore a linker must be selected here to make the situation as close as possible to the ideal one. The linker should be short but guiding suitable stretching orientation of Ring C. Series iv has been chosen in consideration of Ring C orientation, as well as ADMET properties and introduction of possible hydrogen bond.

## 2. Results and discussion

### 2.1. Chemistry

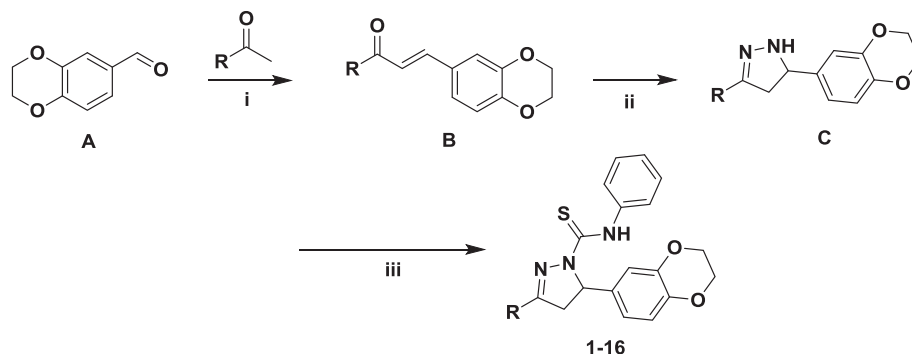
5-(2,3-dihydrobenzo[b][1,4]dioxane-6-yl)-N,3-diaryl-4,5-dihydro-1H-pyrazole-1-carbothioamide derivatives **1–16** were

synthesized and screened for their biological activity. All of them were synthesized and tested for the first time. The general synthesis method and the structures of compounds **1–16** were organized in Scheme 1. They were all prepared in three steps. Firstly, different substituted aromatic ketone on treatment with 2,3-dihydrobenzo[b][1,4]dioxane-6-carbaldehyde in presence of 50% NaOH solution were stirred at room temperature till reactions completed, yielding different analogues of chalcones (**B**). Secondly, hydrazine hydrate was added to participate the cyclization of the obtained powder [34]. Thirdly, phenyl isothiocyanate was added and refluxed, leading to the corresponding target compounds **1–16**. Subsequent purification with recrystallisation was conducted and the refined compounds were finally obtained. All of the synthetic compounds gave satisfactory analytical and spectroscopic data, which were in full accordance with their depicted structures.

### 2.2. Biological activity

Before evaluated for anti-proliferation effect and BRAF inhibitory activity, ADMET properties as a preliminary evaluation for the basic druggability were shown in Fig. 2. Although the linker was chosen strictly, compound **6**, **13**, **14** and **15** might still need possible pharmacokinetics group to improve their logP and PSA (polar surface area) values. All the other compounds were in nice situation and ready for subsequent bioassay.

With a general method, the anti-proliferation and BRAF inhibitory effect was evaluated. To compare the differences in inhibiting BRAF<sup>V600E</sup> and BRAF<sup>WT</sup>, the IC<sub>50</sub> values (the half maximal inhibitory concentration of BRAF mediated MEK phosphorylation) were shown together with GI<sub>50</sub> values (the half maximal inhibitory concentration of cell growth) of cell lines including human melanoma cells A375 (BRAF<sup>V600E</sup> mutated), WM2664 (BRAF<sup>V600E</sup>



**Scheme 1.** General synthesis of compounds (**1–16**). Reagents and Conditions: i) EtOH, 50% NaOH, TLC; ii)  $\text{N}_2\text{H}_4 \cdot \text{H}_2\text{O}$ , EtOH, NaOH, reflux, 4 h; iii) Phenyl isothiocyanate, EtOH, reflux, 4–6 h.

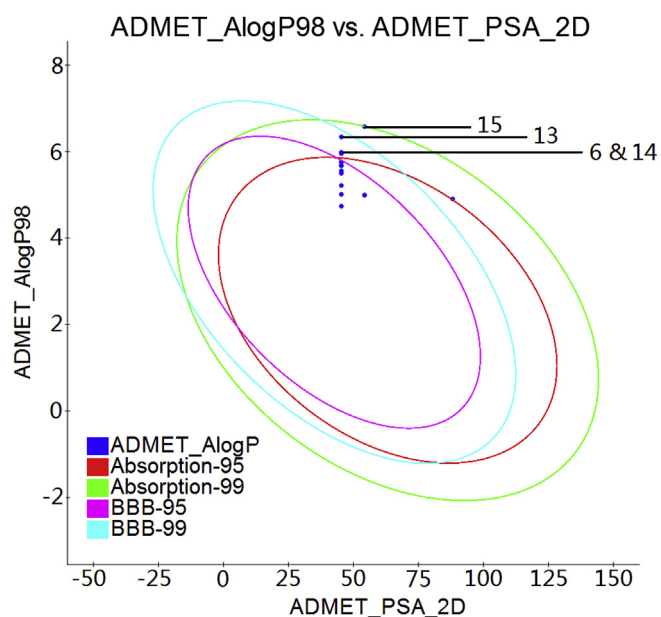


**Fig. 2.** ADMET properties predicted for the sixteen compounds **1–16**. Compounds located inside the innermost oval are better for this parameter. The four compounds outside the innermost oval were **6**, **13**, **14** and **15**.

mutated) and WM1361 ( $\text{BRAF}^{\text{WT}}$ ), human colon cancer cells HT29 ( $\text{BRAF}^{\text{V600E}}$  mutated) and HCT116 ( $\text{BRAF}^{\text{WT}}$ ). As presented in Table 1, a majority of this series indicated potent  $\text{BRAF}^{\text{V600E}}$  inhibitory activity, with a welcome change in weakening  $\text{BRAF}^{\text{WT}}$  inhibitory effect. This result inferred the rotation of backbone and redesign of linker might lead to desirable orientation.

The anti-proliferation effect showed positive correlation with the BRAF inhibitory activity. Representatives including **15** ( $\text{IC}_{50} = 0.01 \mu\text{M}$  for  $\text{BRAF}^{\text{V600E}}$ ;  $\text{GI}_{50} = 0.35 \mu\text{M}$  for A375), **4** ( $\text{IC}_{50} = 0.05 \mu\text{M}$  for  $\text{BRAF}^{\text{V600E}}$ ;  $\text{GI}_{50} = 0.47 \mu\text{M}$  for A375) and **12** ( $\text{IC}_{50} = 0.06 \mu\text{M}$  for  $\text{BRAF}^{\text{V600E}}$ ;  $\text{GI}_{50} = 0.52 \mu\text{M}$  for A375) all displayed comparable activity with the positive controls Vemurafenib ( $\text{IC}_{50} = 0.03 \mu\text{M}$  for  $\text{BRAF}^{\text{V600E}}$ ;  $\text{GI}_{50} = 0.95 \mu\text{M}$  for A375). However, only **12** indicated fine selectivity for  $\text{BRAF}^{\text{V600E}}$  over  $\text{BRAF}^{\text{WT}}$  and this kind of selectivity retained in corresponding cell lines.

After bioassay results being compared, preliminary SAR studies on  $\text{BRAF}^{\text{V600E}}$  were provided. Initially, when Ring B was pushing the A-C plane, substitutes on the A-C plane might face limit of space extension and electronic changing. For *para*-position on Ring A, a preliminary tendency might be induced that substitutes with smaller steric or electronic influence seemed better, with the corresponding order as  $-\text{Br}$  (**4**,  $\text{IC}_{50} = 0.05 \mu\text{M}$ )  $>$   $-\text{H}$  (**1**,  $\text{IC}_{50} = 0.82 \mu\text{M}$ )  $>$   $-\text{Me}$  (**5**,  $\text{IC}_{50} = 4.28 \mu\text{M}$ )  $>$   $-\text{F}$  (**2**,  $\text{IC}_{50} = 11.1 \mu\text{M}$ )  $>$   $-\text{CF}_3$  (**6**,  $\text{IC}_{50} = 29.5 \mu\text{M}$ )  $>$   $-\text{NO}_2$  (**8**,  $\text{IC}_{50} = 57.2 \mu\text{M}$ )  $>$   $-\text{SMe}$  (**7**,  $\text{IC}_{50} = 84.3 \mu\text{M}$ )  $>$   $-\text{Cl}$  (**3**,  $\text{IC}_{50} = 135 \mu\text{M}$ ). However,  $-\text{OBn}$  (**15**,  $\text{IC}_{50} = 0.01 \mu\text{M}$ ) group inferred superb potency, which might be brought by stretching or reversing the backbone (according to the molecular overlap in Fig. 3) as

**Table 1**  
BRAF inhibitory and anti-proliferation activity of the synthesized compounds (**1–16**).

Code	$\text{IC}_{50}$ ( $\mu\text{M}$ ) $\text{BRAF}^{\text{V600E}}$	$\text{IC}_{50}$ ( $\mu\text{M}$ ) $\text{BRAF}^{\text{WT}}$	$\text{GI}_{50}$ ( $\mu\text{M}$ ) A375	$\text{GI}_{50}$ ( $\mu\text{M}$ ) WM2664	$\text{GI}_{50}$ ( $\mu\text{M}$ ) WM1361	$\text{GI}_{50}$ ( $\mu\text{M}$ ) HT29	$\text{GI}_{50}$ ( $\mu\text{M}$ ) HCT116
<b>1</b>	$0.82 \pm 0.07$	$21.3 \pm 1.96$	$1.85 \pm 0.15$	$3.18 \pm 0.29$	$58.5 \pm 5.43$	$6.63 \pm 0.76$	$57.6 \pm 5.33$
<b>2</b>	$11.1 \pm 1.02$	$23.1 \pm 2.03$	$15.7 \pm 1.28$	$22.5 \pm 1.98$	$65.3 \pm 6.22$	$37.6 \pm 5.31$	$61.2 \pm 5.87$
<b>3</b>	$135 \pm 11.4$	$>200$	$195 \pm 18.5$	$>200$	$>200$	$187 \pm 15.6$	$>200$
<b>4</b>	$0.05 \pm 0.002$	$18.7 \pm 1.29$	$0.47 \pm 0.04$	$0.87 \pm 0.07$	$37.5 \pm 3.31$	$2.58 \pm 0.22$	$32.1 \pm 3.01$
<b>5</b>	$4.28 \pm 0.36$	$>200$	$6.32 \pm 0.58$	$10.3 \pm 1.01$	$>200$	$19.5 \pm 1.87$	$>200$
<b>6</b>	$29.5 \pm 1.85$	$35.6 \pm 3.14$	$43.5 \pm 3.97$	$52.4 \pm 4.87$	$123 \pm 12.1$	$97.5 \pm 8.67$	$112 \pm 10.3$
<b>7</b>	$84.3 \pm 6.37$	$156 \pm 12.7$	$159 \pm 14.2$	$197 \pm 16.8$	$187 \pm 16.8$	$>200$	$193 \pm 17.2$
<b>8</b>	$57.2 \pm 4.71$	$>200$	$78.1 \pm 7.32$	$105 \pm 9.86$	$>200$	$153 \pm 13.8$	$>200$
<b>9</b>	$>200$	$124 \pm 10.3$	$>200$	$>200$	$>200$	$>200$	$195 \pm 19.3$
<b>10</b>	$12.1 \pm 0.95$	$>200$	$20.3 \pm 1.96$	$25.8 \pm 2.14$	$>200$	$30.5 \pm 2.95$	$>200$
<b>11</b>	$>200$	$95.9 \pm 8.36$	$>200$	$>200$	$153 \pm 14.8$	$>200$	$138 \pm 12.8$
<b>12</b>	$0.06 \pm 0.003$	$>200$	$0.52 \pm 0.05$	$1.38 \pm 0.11$	$>200$	$2.92 \pm 0.24$	$>200$
<b>13</b>	$30.6 \pm 2.98$	$39.3 \pm 3.41$	$41.9 \pm 4.02$	$58.7 \pm 5.62$	$122 \pm 11.5$	$95.3 \pm 9.17$	$125 \pm 12.2$
<b>14</b>	$38.9 \pm 3.12$	$48.9 \pm 3.98$	$61.3 \pm 5.85$	$70.5 \pm 6.62$	$148 \pm 14.2$	$133 \pm 10.5$	$144 \pm 10.8$
<b>15</b>	$0.01 \pm 0.001$	$5.23 \pm 0.51$	$0.35 \pm 0.03$	$0.42 \pm 0.03$	$8.23 \pm 0.80$	$0.86 \pm 0.08$	$8.53 \pm 0.74$
<b>16</b>	$78.3 \pm 6.82$	$5.21 \pm 0.49$	$121 \pm 10.3$	$154 \pm 12.7$	$7.96 \pm 0.73$	$188 \pm 17.2$	$8.19 \pm 0.81$
Vemurafenib	$0.03 \pm 0.003$	$0.18 \pm 0.01$	$0.95 \pm 0.08$	$0.21 \pm 0.02$	$20.8 \pm 1.95$	$1.88 \pm 0.15$	$25.2 \pm 2.18$

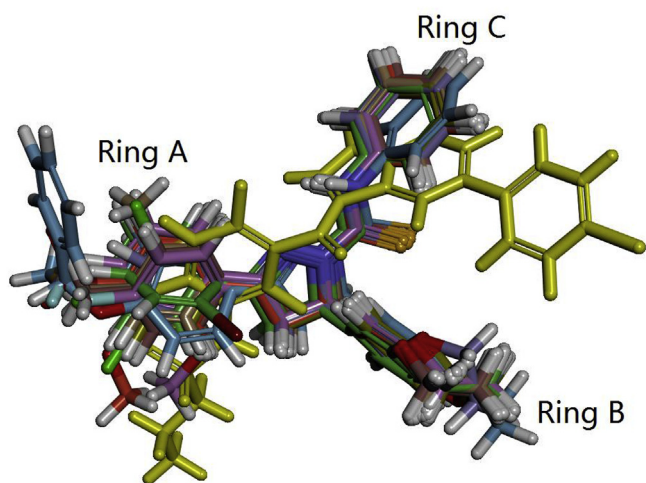


**Fig. 3.** Molecular overlap of compounds **1–16** with Vemurafenib (in pure color). Ring A and C were almost in one plane while Ring B indicated an angle with this plane. The backbone of **15** was stretching at Ring A and reversing at Ring B. (For interpretation of the references to color in this figure legend, the reader is referred to the Web version of this article.)

mentioned in our previous work [30]. For *meta*-position and *ortho*-position, a clear inference was that electron-donating groups might increase the potency and selectivity for BRAF<sup>V600E</sup> whereas electron-withdrawing groups might ruin them. The corresponding example for *meta*-position is -OMe (**12**, IC<sub>50</sub> = 0.06 μM) > -Cl (**11**, IC<sub>50</sub> > 200 μM) and that for *ortho*-position is -OMe (**10**, IC<sub>50</sub> = 12.1 μM) > -Br (**9**, IC<sub>50</sub> > 200 μM). Secondly, multi substitutes on both *ortho*- and *meta*-positions suggested moderated BRAF<sup>V600E</sup> inhibitory activity but no specific selectivity from BRAF<sup>WT</sup>. Thirdly, a heterocyclic ring (here it was thiophene) also seemed worse than benzene ring due to weakening BRAF<sup>V600E</sup> inhibitory effect but increasing BRAF<sup>WT</sup> inhibiting. Thus, keeping Ring A substitutes in low-impact status or throwing it out the pocket seemed favorable for potent inhibition of BRAF<sup>V600E</sup>, while **12** revealed a corner of the iceberg for introducing considerable selectivity.

Compound **4**, **12** and **15** were chosen as representatives for further kinase inhibitory selectivity evaluation against CRAF (also called RAF1), MEK, JNK1 and p38α. As shown in Table 2, only **12** provided superb selectivity for BRAF<sup>V600E</sup> against other kinases (especially CRAF, and BRAF<sup>WT</sup> in Table 1). **4** and **15** were both active against BRAF<sup>V600E</sup> but regrettably potent against BRAF<sup>WT</sup> and relative kinases such as CRAF and JNK1. Meanwhile, these representatives all suggested low cytotoxicity against HEK293T (human embryonic kidney cell line) and LO2 (human embryonic liver cell line) cells. Through the screening of broaden selectivity and cytotoxicity, **12** was chosen for further study.

Flow cytometry analysis was conducted to convince that the anti-proliferative activity was correlated to apoptosis. As shown in Fig. 4, compound **12** could induce apoptosis of A375 cells. When the concentration of **12** was settled as 2 μM except control, the percentage of apoptotic cells increased as time varies (24, 48 and 72 h). When treated with increasing concentrations of **12** (0–20 μM) for

24 h, the percentage of apoptotic cells inferred a significant increase in a dose-dependent manner. Meanwhile, G2-block arrest of A375 was observed in a time-dependent manner with the concentration of **12** settled as 2 μM and in a dose-dependent manner with the incubation time settled as 24 h. Thus, **12** could enhance the accumulation of cells in G2/M phase.

BRAF<sup>V600E</sup> inhibitors should block the phosphorylated level downstream MEK and ERK. Thus, the blocking effect of compound **12** on phosphorylation of MEK and ERK from A375 (BRAF<sup>V600E</sup>) and WM1361 (BRAF<sup>WT</sup>) cell lines was evaluated. For BRAF<sup>V600E</sup> group, cells were treated with different concentrations (0 μM, 0.05 μM, 0.1 μM and 0.5 μM) of compound **12**. As shown in Fig. 5, **12** could suppress the phosphorylation of MEK and ERK from A375 cell line in a dose-dependent manner (Fig. 5A and B), being close to Vemurafenib in literature. However, for BRAF<sup>WT</sup> group (Fig. 5D and E), no such effect was observed with higher concentrations (0 μM, 0.5 μM, 1 μM and 5 μM) of **12**. In both groups, no suppression of total MEK1/2 or ERK1/2 levels were observed. Compound **15**, as a contrast, also suggested blocking effect on pMEK from A375 cells (Fig. 5C).

A375 cells were subcutaneously inoculated into right flank of nude mice to evaluate the antitumor effect of compound **12**. The mice were randomized into 4 groups including vehicle control, Vemurafenib (5 mg/kg) and **12** (5 and 10 mg/kg). The compounds were intraperitoneally administered every second day for 14 days. Body weight were monitored and recorded every two days and did not show obvious decrease (Fig. 6A). This result supported the safety. Tumors were taken out and weighed on day 15. This parameter inferred evidence for the antitumor efficacy. The results in Fig. 6B suggested the average weight of tumors in control group (0.79 ± 0.061 g) was 2-fold more than that of **12**-treated (10 mg/kg) group (0.38 ± 0.029 g). Compound **12** exhibited comparable antitumor efficacy with the positive control Vemurafenib (5 mg/kg, 0.41 ± 0.031 g).

### 2.3. Molecular docking

Molecular docking was performed to visualize the possible binding models using CDOCKER protocol in Discovery Studio 3.5 (Discovery Studio 3.5, Accelrys, Inc. San Diego, CA). The crystal structures of BRAF<sup>V600E</sup> (PDB Code: 1UWJ) and BRAF<sup>WT</sup> (PDB Code: 1UWH) were chosen [20]. The receptor and ligands were prepared and the binding site was defined. The CDOCKER Interaction Energy (interaction energy between the ligand and the receptor, shown in Table 3) agreed with the BRAF inhibitory trend for all the synthesized compounds. The 2D maps of compound **4**, **12**, **15** into BRAF<sup>V600E</sup> and **15** into BRAF<sup>WT</sup> were depicted in Fig. 7.

The binding pattern of compound **4**, **12**, **15** into BRAF<sup>V600E</sup> was similar to previous researches with PHE582 (PHE583 as previously mentioned) between Ring A and Ring C. Especially for **4** and **12**, they retained typical π–π interactions between Ring A/C and TRP530 and π–cation interactions between Ring B and LYS482. However, the new hydrogen bond (**4**: O···H-N, 2.13 Å, 118.80°; **12**: O···H-N, 2.10 Å, 118.78°) between -NH- on linker and PHE594 might enhance the inhibitory activity against BRAF<sup>V600E</sup>.

**Table 2**  
Selectivity (against CRAF, MEK1/2, JNK1 and p38α) and Cytotoxicity (against HEK293T and LO2 cell lines) of representative compounds (**4**, **12** and **15**).

Code	IC <sub>50</sub> (μM) CRAF	IC <sub>50</sub> (μM) MEK1/2	IC <sub>50</sub> (μM) JNK1	IC <sub>50</sub> (μM) p38α	GI <sub>50</sub> (μM) HEK293T	GI <sub>50</sub> (μM) LO2
<b>4</b>	17.6 ± 1.58	188 ± 16.5	93.6 ± 9.11	>200	152 ± 14.8	188 ± 16.2
<b>12</b>	>200	195 ± 18.9	>200	>200	>200	>200
<b>15</b>	3.15 ± 0.30	176 ± 15.7	88.9 ± 8.42	>200	175 ± 15.1	>200

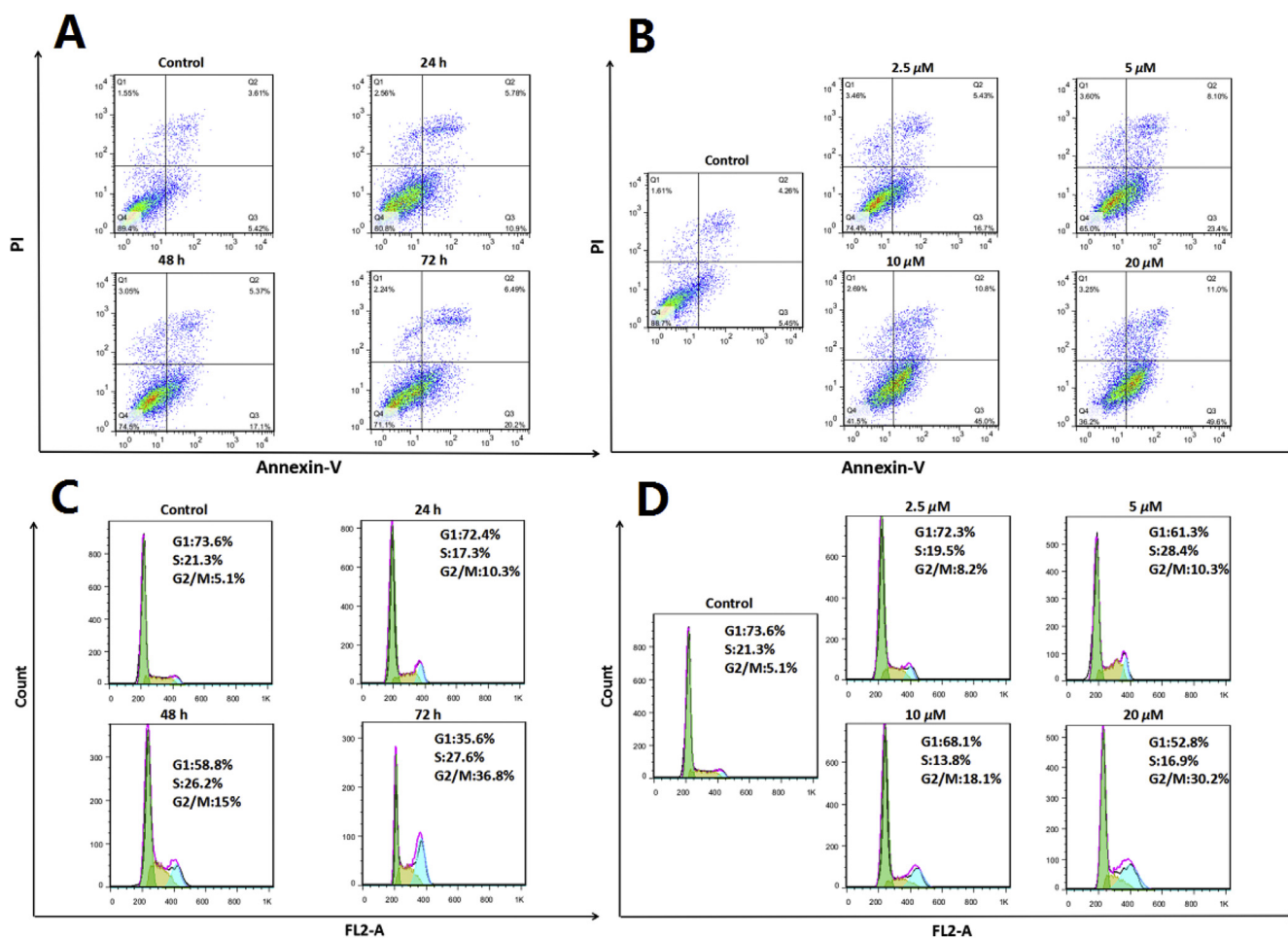


**Fig. 4.** Flow cytometry analysis of compound **12** on A375 cell line. (A) Time-dependent cell apoptosis with 2  $\mu$ M compound **12**; (B) Dose-dependent cell apoptosis for 24 h; (C) Time-dependent G2-block arrest of A375 with 2  $\mu$ M compound **12**; (D) Dose-dependent G2-block arrest of A375 for 24 h.

Meanwhile, compound **15** stretched its Ring A substitute out the pocket to interact with residues including LYS600 and SER601, which might bring favorable effect without stick to the typical pattern. As for binding pattern into BRAF<sup>WT</sup>, HIS573 seemed to be a key residue for this series. Compound **15** suggested  $\pi$ - $\pi$  and  $\pi$ -cation interactions here while **4** indicated weaker binding situation. Compound **12** even failed to be docked into BRAF<sup>WT</sup>. These results agreed with their BRAF<sup>WT</sup> inhibiting performance. Besides, the 3D binding situation and receptor surface model with **12** in BRAF<sup>V600E</sup> in Fig. 8 all inferred that **12** was deeply occupation into the active pocket. Herein, two new hints were found. One was involving PHE594 of BRAF<sup>V600E</sup> to enhance inhibition, while the other was evading HIS573 of BRAF<sup>WT</sup> to introduce selectivity.

### 3. Conclusions

In summary, a series of selective BRAF<sup>V600E</sup> inhibitory agents (Compound **1**–**16**) have been designed and synthesized. Inheriting the ABC-ring system and 1,4-benzodioxane group, cautious rotation and linker choice maintained the interactions with key residues and brought selectivity. **15**, **4** and **12** all displayed comparable activity with the positive control Vemurafenib. Remarkably, **12** indicated fine selectivity on BRAF<sup>V600E</sup> over BRAF<sup>WT</sup> at both kinase and cell levels. Flow cytometry analysis verified the apoptosis induction and western blot convinced the kinase inhibitory effect. Docking simulation implied the binding pattern including PHE582, LYS482 and TRP530. It provided further hints of involving PHE594

(BRAF<sup>V600E</sup>) to enhance inhibition and evading HIS573 (BRAF<sup>WT</sup>) to introduce selectivity. This work might infer some clues for future development of selective BRAF inhibitors and correlative safe medication.

## 4. Experimental section

### 4.1. Chemistry

#### 4.1.1. General

All commercially available chemicals were used as received without further purification. Melting points were determined on a WRS-1C digital melting point apparatus and were uncorrected. <sup>1</sup>H NMR and <sup>13</sup>C NMR spectra were recorded on a Bruker Avance II 600 spectrometer. Shifts are reported in parts per million based on residual solvent peaks (for <sup>1</sup>H or <sup>13</sup>C/CDCl<sub>3</sub> or DMSO-*d*<sub>6</sub>). NMR data were resolved with MestreNova software. Mass spectra were obtained from an Agilent 6540 UHD Accurate Mass Q-TOF LC/MS.

#### 4.1.2. General method of synthesis of (E)-Chalcones (B)

Substituted aromatic ketone (1 mmol) was added to 2,3-dihydrobenzo[*b*][1,4] dioxane-6-carbaldehyde (A) (1 mmol) alcohol solution (5 mL). After dissolution, 50% NaOH (0.5 mL) was added. After confirming the completion of the reaction by thin layer chromatography, the sediment was filtered, washed with ethanol and dried to obtain chalcone (B).

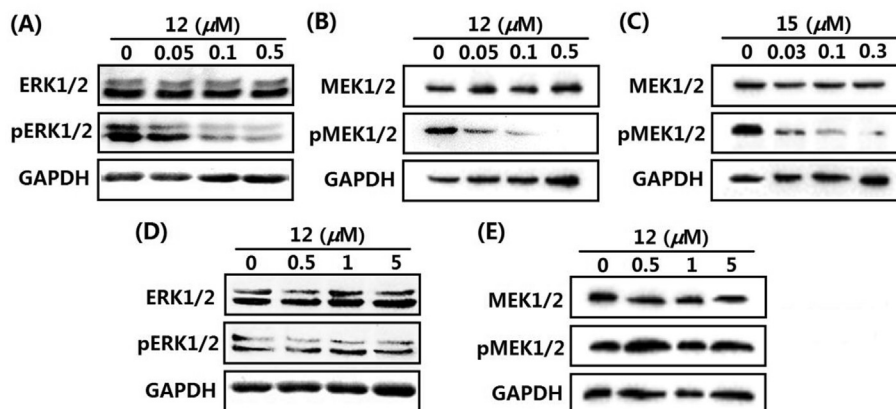


**Fig. 5.** Compound **12** blocked the ERK pathway in A375 cells but the blocking was not obvious in WM1361 cells. **12** inhibited the phosphorylation of ERK (A) and MEK (B) in A375 cells expressing BRAF<sup>V600E</sup>; **15** inhibited the phosphorylation of MEK (C) in A375 cells expressing BRAF<sup>V600E</sup>. The inhibition of **12** with higher concentrations on the phosphorylation of ERK (D) and MEK (E) was not obvious in WM1361 cells expressing BRAF<sup>WT</sup>.

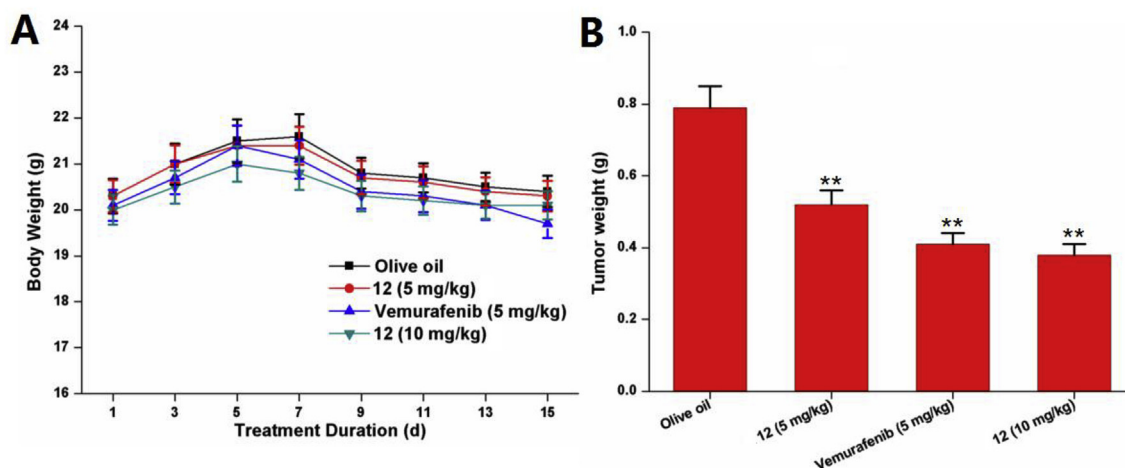


**Fig. 6.** Compound **12** indicated low toxicity and potent antitumor effect in xenografts of A375 cell line. (A) Body weight monitored and recorded every two days; (B) Tumor weight on day 15 of treatment.

**Table 3**  
The CDocker Interaction Energy of the synthesized compounds (**1–16**).

Code	-CDocker Interaction Energy (kcal/mol)	Code	-CDocker Interaction Energy (kcal/mol)
<b>1</b>	48.2530	<b>9</b>	33.5368
<b>2</b>	46.0991	<b>10</b>	45.4921
<b>3</b>	40.9463	<b>11</b>	39.2084
<b>4</b>	50.9873	<b>12</b>	50.6685
<b>5</b>	47.3400	<b>13</b>	44.0407
<b>6</b>	43.3818	<b>14</b>	42.6499
<b>7</b>	41.7242	<b>15</b>	52.9371
<b>8</b>	42.3797	<b>16</b>	42.0848

#### 4.1.3. General method of synthesis of (E)-3-(2,3-dihydrobenzo[b][1,4]dioxane-6-yl)-1-phenylprop-2-en-1-one (**C1–C16**)

The solution of appropriate chalcones (**B**, 1 mmol) and hydrazine hydrate (2 mmol) in ethanol (5 mL) was refluxed for 4 h. The mixture was evaporated to dryness and the residue was crystallized from suitable solvents to receive the target compounds **C1–C16**.

#### 4.1.4. General method of synthesis of 5-(2,3-dihydrobenzo[b][1,4]dioxane-6-yl)-N,3-diphenyl-4,5-dihydro-1H-pyrazole-1-carbothioamide (**1–16**)

To the stirred solution of compounds (**C1–C16**, 1 mmol) in

absolute ethanol, was added substituted phenyl isothiocyanates (2 mmol) and refluxed for 4–6 h. The crude product was filtered, washed with petroleum ether, dried, and was recrystallized from methanol to afford the title compounds **1–16**.

**4.1.4.1.** 5-(2,3-dihydrobenzo[b][1,4]dioxane-6-yl)-N,3-diphenyl-4,5-dihydro-1H-pyrazole-1-carbothioamide (**1**). Orange solid; mp 135–137 °C; yield: 77%; <sup>1</sup>H NMR (400 MHz, CDCl<sub>3</sub>) δ 9.28 (s, 1H), 7.79 (d, J = 7.5 Hz, 2H), 7.67 (d, J = 8.0 Hz, 2H), 7.49–7.47 (m, 3H), 7.38 (t, J = 7.6 Hz, 2H), 7.20 (t, J = 7.4 Hz, 1H), 6.86–6.78 (m, 3H), 6.12 (dd, J = 11.4, 3.1 Hz, 1H), 4.25 (s, 4H), 3.85 (dd, J = 17.7, 11.4 Hz, 1H), 3.24 (dd, J = 17.6, 3.2 Hz, 1H); <sup>13</sup>C NMR (151 MHz, DMSO) δ 173.81, 155.95, 143.65, 142.55, 141.24, 140.00, 136.42, 130.75, 128.52, 128.42, 128.00, 127.78, 125.27, 118.21, 117.60, 114.38, 64.51, 64.42, 63.12, 42.62; HRMS (ESI-TOF) m/z: [M+H]<sup>+</sup> Calcd for C<sub>24</sub>H<sub>22</sub>N<sub>3</sub>O<sub>2</sub>S 416.1354, Found 416.1352.

**4.1.4.2.** 5-(2,3-dihydrobenzo[b][1,4]dioxane-6-yl)-3-(4-fluorophenyl)-N-phenyl-4,5-dihydro-1H-pyrazole-1-carbothioamide (**2**). Pale yellow solid; mp 186–187 °C; yield: 66%; <sup>1</sup>H NMR (600 MHz, DMSO-d<sub>6</sub>) δ 10.18 (s, 1H), 8.07 (dd, J = 8.4, 5.6 Hz, 2H), 7.56 (d, J = 7.8 Hz, 2H), 7.36–7.33 (m, 4H), 7.17 (t, J = 7.3 Hz, 1H), 6.81 (d, J = 8.1 Hz, 1H), 6.67–6.65 (m, 2H), 5.94 (dd, J = 11.2, 2.9 Hz, 1H), 4.21 (s, 4H), 3.90 (dd, J = 18.1, 11.4 Hz, 1H), 3.21 (dd, J = 18.1, 3.1 Hz,

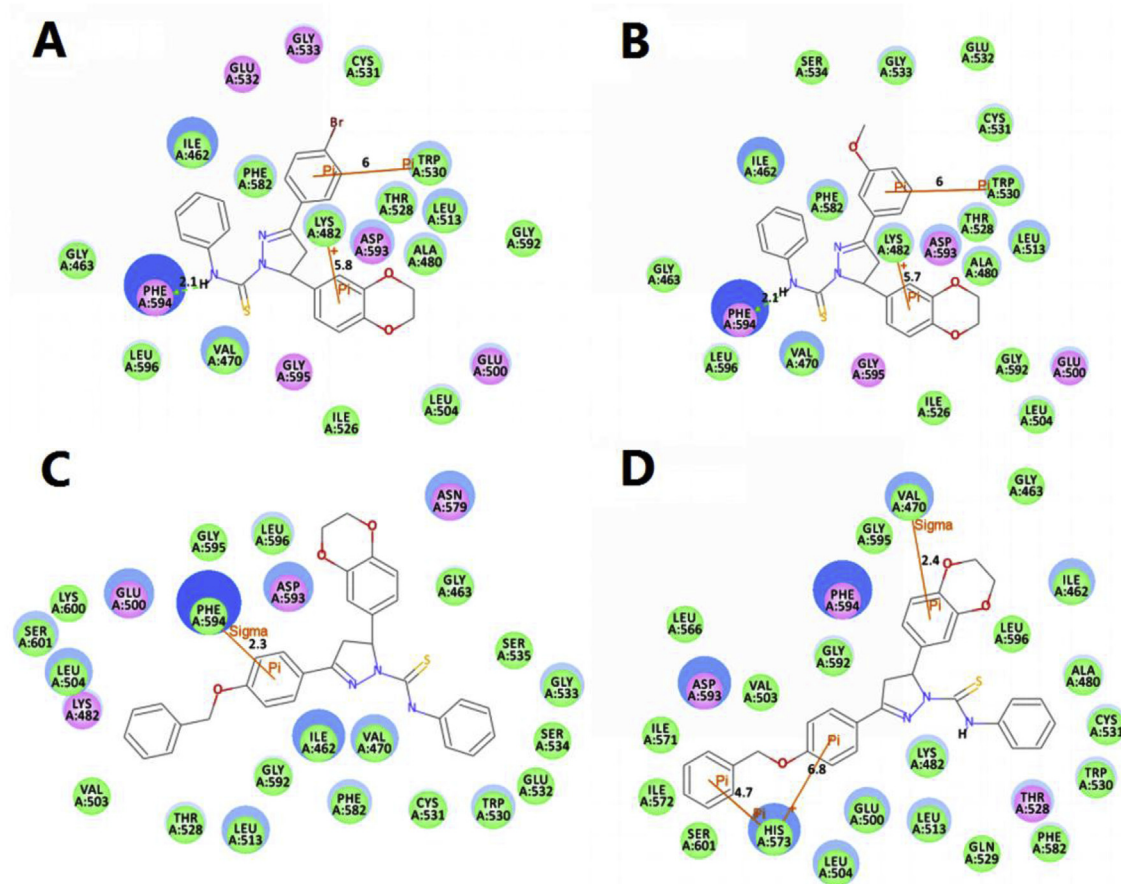


**Fig. 7.** The 2D docking models of representative compounds. (A) Compound **4** into BRAF<sup>V600E</sup>; (B) Compound **12** into BRAF<sup>V600E</sup>; (C) Compound **15** into BRAF<sup>V600E</sup>; (D) Compound **15** into BRAF<sup>WT</sup>. The H-bonds are displayed as dotted lines. The  $\pi$ -cation,  $\pi$ - $\pi$  and  $\pi$ -sigma interactions are shown as orange lines. Interactions with typical PHE582, LYS482 and TRP530 were retained. New found interactions included PHE594 of BRAF<sup>V600E</sup> and HIS573 of BRAF<sup>WT</sup>. (For interpretation of the references to color in this figure legend, the reader is referred to the Web version of this article.)

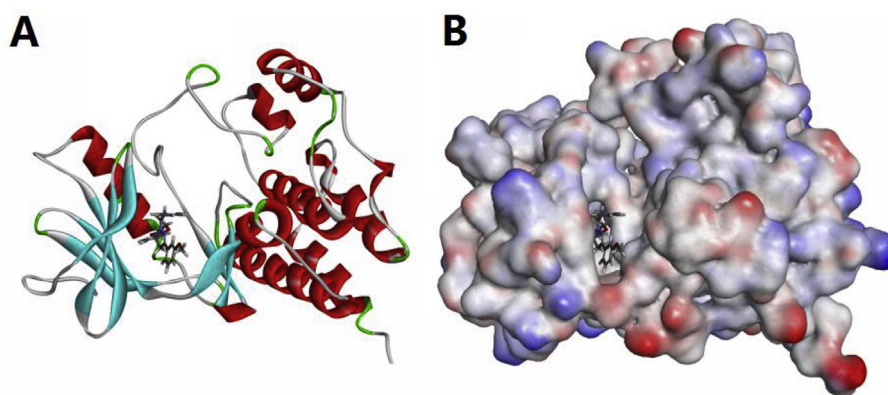


**Fig. 8.** (A) The 3D binding situation of compound **12** into BRAF<sup>V600E</sup>; (B) The receptor surface model with **12** in BRAF<sup>V600E</sup>.

1H); <sup>13</sup>C NMR (151 MHz, DMSO)  $\delta$  174.11, 155.04, 143.65, 142.87, 139.97, 136.22, 130.38, 130.32, 128.49, 127.94, 127.86, 127.69, 125.36, 118.68, 117.63, 116.33, 116.19, 114.48, 64.55, 64.44, 63.34, 42.55; HRMS (ESI-TOF)  $m/z$ : [M+H]<sup>+</sup> Calcd for C<sub>24</sub>H<sub>21</sub>FN<sub>3</sub>O<sub>2</sub>S 434.1260, Found 434.1262.

4.1.4.3. 3-(4-chlorophenyl)-5-(2,3-dihydrobenzo[b][1,4]dioxane-6-yl)-N-phenyl-4,5-dihydro-1H-pyrazole-1-carbothioamide (**3**). Pale yellow solid; mp 189–190 °C; yield: 75%; <sup>1</sup>H NMR (600 MHz,

DMSO-*d*<sub>6</sub>)  $\delta$  10.21 (s, 1H), 8.02 (d,  $J$  = 8.6 Hz, 2H), 7.57–7.55 (m, 4H), 7.35 (t,  $J$  = 7.7 Hz, 2H), 7.17 (t,  $J$  = 7.4 Hz, 1H), 6.81 (d,  $J$  = 8.1 Hz, 1H), 6.67–6.64 (m, 2H), 5.95 (dd,  $J$  = 11.3, 3.2 Hz, 1H), 4.21 (s, 4H), 3.90 (dd,  $J$  = 18.1, 11.4 Hz, 1H), 3.20 (dd,  $J$  = 18.1, 3.4 Hz, 1H); <sup>13</sup>C NMR (151 MHz, DMSO)  $\delta$  174.02, 157.24, 143.24, 142.63, 140.01, 139.14, 136.46, 130.08, 128.88, 128.51, 127.16, 125.48, 125.32, 118.68, 117.63, 115.55, 64.55, 64.44, 63.22, 42.33; HRMS (ESI-TOF)  $m/z$ : [M+H]<sup>+</sup> Calcd for C<sub>24</sub>H<sub>21</sub>ClN<sub>3</sub>O<sub>2</sub>S 450.0964, Found 450.0963.

4.1.4.4. 3-(4-bromophenyl)-5-(2,3-dihydrobenzo[b][1,4]dioxane-6-yl)-N-phenyl-4,5-dihydro-1H-pyrazole-1-carbothioamide (**4**).

Yellow solid; mp 171–173 °C; yield: 72%; <sup>1</sup>H NMR (600 MHz, DMSO-*d*<sub>6</sub>) δ 10.21 (s, 1H), 7.94 (d, *J* = 8.6 Hz, 2H), 7.70 (d, *J* = 8.6 Hz, 2H), 7.55 (d, *J* = 7.6 Hz, 2H), 7.35 (t, *J* = 7.6 Hz, 2H), 7.17 (t, *J* = 7.4 Hz, 1H), 6.81 (d, *J* = 8.2 Hz, 1H), 6.66–6.64 (m, 2H), 5.94 (dd, *J* = 11.2, 3.2 Hz, 1H), 4.20 (s, 4H), 3.90 (dd, *J* = 18.1, 11.4 Hz, 1H), 3.19 (dd, *J* = 18.1, 3.4 Hz, 1H); <sup>13</sup>C NMR (151 MHz, DMSO) δ 174.17, 154.94, 143.65, 142.89, 139.94, 136.18, 132.15, 130.59, 129.81, 128.50, 125.92, 125.37, 124.71, 118.69, 117.63, 114.48, 64.55, 64.44, 63.42, 42.29; HRMS (ESI-TOF) *m/z*: [M+H]<sup>+</sup> Calcd for C<sub>24</sub>H<sub>21</sub>BrN<sub>3</sub>O<sub>2</sub>S 494.0459, Found 494.0461.

4.1.4.5. 5-(2,3-dihydrobenzo[b][1,4]dioxane-6-yl)-N-phenyl-3-(*p*-tolyl)-4,5-dihydro-1H-pyrazole-1-carbothioamide (**5**). Pale yellow solid; mp 144–146 °C; yield: 75%; <sup>1</sup>H NMR (600 MHz, DMSO-*d*<sub>6</sub>) δ 10.12 (s, 1H), 7.89 (d, *J* = 8.2 Hz, 2H), 7.58 (d, *J* = 7.7 Hz, 2H), 7.34 (t, *J* = 7.7 Hz, 2H), 7.30 (d, *J* = 8.0 Hz, 2H), 7.16 (t, *J* = 7.4 Hz, 1H), 6.81 (d, *J* = 8.2 Hz, 1H), 6.67–6.64 (m, 2H), 5.93 (dd, *J* = 11.1, 3.1 Hz, 1H), 4.20 (s, 4H), 3.88 (dd, *J* = 18.0, 11.3 Hz, 1H), 3.17 (dd, *J* = 18.1, 3.3 Hz, 1H), 2.37 (s, 3H); <sup>13</sup>C NMR (151 MHz, DMSO) δ 173.91, 156.05, 143.64, 142.85, 141.24, 140.01, 136.29, 129.75, 128.53, 128.46, 127.89, 125.77, 125.27, 118.67, 117.61, 114.46, 64.55, 64.44, 63.12, 42.52, 21.58; HRMS (ESI-TOF) *m/z*: [M+H]<sup>+</sup> Calcd for C<sub>25</sub>H<sub>24</sub>N<sub>3</sub>O<sub>2</sub>S 430.1511, Found 430.1513.

4.1.4.6. 5-(2,3-dihydrobenzo[b][1,4]dioxane-6-yl)-N-phenyl-3-(4-(trifluoromethyl)phenyl)-4,5-dihydro-1H-pyrazole-1-carbothioamide (**6**). White solid; mp 164–165 °C; yield: 64%; <sup>1</sup>H NMR (600 MHz, DMSO-*d*<sub>6</sub>) δ 10.31 (s, 1H), 8.21 (d, *J* = 8.2 Hz, 2H), 7.85 (d, *J* = 8.3 Hz, 2H), 7.55 (d, *J* = 7.7 Hz, 2H), 7.36 (t, *J* = 7.6 Hz, 2H), 7.18 (t, *J* = 7.4 Hz, 1H), 6.81 (d, *J* = 8.4 Hz, 1H), 6.68–6.67 (m, 2H), 5.98 (dd, *J* = 11.7, 3.3 Hz, 1H), 4.21 (s, 4H), 3.95 (dd, *J* = 18.2, 11.5 Hz, 1H), 3.25 (dd, *J* = 18.2, 3.5 Hz, 1H); <sup>13</sup>C NMR (151 MHz, DMSO) δ 174.56, 154.39, 143.67, 142.92, 139.91, 136.14, 135.32, 128.53, 128.51, 126.05, 126.00, 125.98, 125.54, 125.42, 123.62, 118.71, 117.65, 114.51, 64.55, 64.44, 63.59, 42.33, 40.52; HRMS (ESI-TOF) *m/z*: [M+H]<sup>+</sup> Calcd for C<sub>24</sub>H<sub>21</sub>F<sub>3</sub>N<sub>3</sub>O<sub>2</sub>S 484.1228, Found 484.1226.

4.1.4.7. 5-(2,3-dihydrobenzo[b][1,4]dioxane-6-yl)-3-(4-(methylthio)phenyl)-N-phenyl-4,5-dihydro-1H-pyrazole-1-carbothioamide (**7**). Pale yellow solid; mp 165–167 °C; yield: 75%; <sup>1</sup>H NMR (600 MHz, DMSO-*d*<sub>6</sub>) δ 10.14 (s, 1H), 7.91 (d, *J* = 8.2 Hz, 2H), 7.58 (d, *J* = 7.8 Hz, 2H), 7.36–7.33 (m, 4H), 7.16 (t, *J* = 7.3 Hz, 1H), 6.81 (d, *J* = 8.0 Hz, 1H), 6.67–6.66 (m, 2H), 5.94 (dd, *J* = 10.9, 2.1 Hz, 1H), 4.20 (s, 4H), 3.87 (dd, *J* = 18.0, 11.4 Hz, 1H), 3.17 (dd, *J* = 17.9, 2.3 Hz, 1H), 2.53 (s, 3H); <sup>13</sup>C NMR (151 MHz, DMSO) δ 173.87, 155.64, 143.65, 142.86, 142.56, 139.99, 136.27, 128.48, 128.27, 127.41, 125.79, 125.31, 118.68, 117.62, 114.48, 64.56, 64.44, 63.19, 42.43, 40.48; HRMS (ESI-TOF) *m/z*: [M+H]<sup>+</sup> Calcd for C<sub>25</sub>H<sub>24</sub>N<sub>3</sub>O<sub>2</sub>S<sub>2</sub> 462.1231, Found 462.1232.

4.1.4.8. 5-(2,3-dihydrobenzo[b][1,4]dioxane-6-yl)-3-(4-nitrophenyl)-N-phenyl-4,5-dihydro-1H-pyrazole-1-carbothioamide (**8**). Red solid; mp 183–184 °C; yield: 56%; <sup>1</sup>H NMR (600 MHz, DMSO-*d*<sub>6</sub>) δ 10.38 (s, 1H), 8.32–8.24 (m, 4H), 7.54 (d, *J* = 7.6 Hz, 2H), 7.36 (t, *J* = 7.6 Hz, 2H), 7.19 (t, *J* = 7.4 Hz, 1H), 6.82 (d, *J* = 8.6 Hz, 1H), 6.68–6.66 (m, 2H), 5.99 (dd, *J* = 11.5, 3.4 Hz, 1H), 4.21 (s, 4H), 3.96 (dd, *J* = 18.2, 11.6 Hz, 1H), 3.26 (dd, *J* = 18.1, 3.5 Hz, 1H); <sup>13</sup>C NMR (151 MHz, DMSO) δ 173.99, 154.36, 143.92, 142.87, 139.93, 136.22, 135.44, 128.33, 128.31, 126.21, 126.00, 125.98, 125.26, 125.20, 123.82, 118.54, 117.26, 114.33, 64.55, 64.44, 63.29, 42.33; HRMS (ESI-TOF) *m/z*: [M+H]<sup>+</sup> Calcd for C<sub>24</sub>H<sub>21</sub>N<sub>4</sub>O<sub>4</sub>S 461.1205, Found 461.1206.

4.1.4.9. 3-(2-bromophenyl)-5-(2,3-dihydrobenzo[b][1,4]dioxane-6-yl)-N-phenyl-4,5-dihydro-1H-pyrazole-1-carbothioamide (**9**).

Pale yellow solid; mp 147–149 °C; yield: 71%; <sup>1</sup>H NMR (600 MHz, DMSO-*d*<sub>6</sub>) δ 10.00 (s, 1H), 7.90 (dd, *J* = 7.8, 1.6 Hz, 1H), 7.76 (d, *J* = 8.0 Hz, 1H), 7.57 (d, *J* = 7.7 Hz, 2H), 7.51 (t, *J* = 7.1 Hz, 1H), 7.42 (t, *J* = 7.7 Hz, 1H), 7.32 (t, *J* = 7.6 Hz, 2H), 7.14 (t, *J* = 7.4 Hz, 1H), 6.84–6.82 (m, 1H), 6.73–6.71 (m, 2H), 5.96 (dd, *J* = 11.3, 3.2 Hz, 1H), 4.22 (s, 4H), 4.09 (dd, *J* = 18.2, 11.5 Hz, 1H), 3.25 (dd, *J* = 18.2, 3.4 Hz, 1H); <sup>13</sup>C NMR (151 MHz, DMSO) δ 174.55, 153.99, 143.42, 142.86, 139.80, 136.24, 135.32, 128.63, 128.51, 126.02, 126.00, 125.88, 125.52, 125.48, 123.53, 118.68, 117.66, 114.52, 64.42, 64.40, 63.58, 42.60; HRMS (ESI-TOF) *m/z*: [M+H]<sup>+</sup> Calcd for C<sub>24</sub>H<sub>21</sub>BrN<sub>3</sub>O<sub>2</sub>S 494.0459, Found 494.0461.

4.1.4.10. 5-(2,3-dihydrobenzo[b][1,4]dioxane-6-yl)-3-(2-methoxyphenyl)-N-phenyl-4,5-dihydro-1H-pyrazole-1-carbothioamide (**10**). White solid; mp 164–166 °C; yield: 74%; <sup>1</sup>H NMR (600 MHz, DMSO-*d*<sub>6</sub>) δ 10.07 (s, 1H), 8.26 (dd, *J* = 7.8, 1.7 Hz, 1H), 7.57 (d, *J* = 7.8 Hz, 2H), 7.48 (t, *J* = 7.9, 1H), 7.33 (t, *J* = 7.6 Hz, 2H), 7.16–7.13 (m, 2H), 7.05 (t, *J* = 7.5 Hz, 1H), 6.81 (d, *J* = 8.2 Hz, 1H), 6.67–6.65 (m, 2H), 5.89 (dd, *J* = 11.2, 3.1 Hz, 1H), 4.21 (s, 4H), 3.96 (dd, *J* = 18.7, 11.3 Hz, 1H), 3.82 (s, 3H), 3.22 (dd, *J* = 18.7, 3.2 Hz, 1H); <sup>13</sup>C NMR (151 MHz, DMSO) δ 173.90, 158.86, 155.34, 143.63, 142.82, 140.02, 136.46, 132.84, 129.88, 128.46, 125.66, 125.22, 121.05, 119.83, 118.60, 117.63, 114.38, 112.91, 64.55, 64.43, 63.09, 56.21, 46.09; HRMS (ESI-TOF) *m/z*: [M+H]<sup>+</sup> Calcd for C<sub>25</sub>H<sub>24</sub>N<sub>3</sub>O<sub>3</sub>S 446.1460, Found 446.1459.

4.1.4.11. 3-(3-chlorophenyl)-5-(2,3-dihydrobenzo[b][1,4]dioxane-6-yl)-N-phenyl-4,5-dihydro-1H-pyrazole-1-carbothioamide (**11**). Pale yellow solid; mp 142–146 °C; yield: 63%; <sup>1</sup>H NMR (600 MHz, DMSO-*d*<sub>6</sub>) δ 10.28 (s, 1H), 8.35 (s, 1H), 7.87 (d, *J* = 6.3 Hz, 1H), 7.68 (d, *J* = 6.4 Hz, 1H), 7.54 (d, *J* = 6.3 Hz, 2H), 7.44–7.18 (m, 4H), 6.82–6.65 (m, 3H), 5.95 (d, *J* = 9.7 Hz, 1H), 4.20 (s, 4H), 3.88 (dd, *J* = 17.2, 12.1 Hz, 1H), 3.22 (d, *J* = 17.7, 1H); <sup>13</sup>C NMR (151 MHz, DMSO) δ 174.22, 154.31, 143.46, 142.88, 140.34, 136.24, 135.52, 128.51, 128.06, 126.25, 126.00, 125.97, 125.54, 125.46, 123.22, 118.35, 117.55, 114.21, 64.64, 64.34, 63.58, 42.36; HRMS (ESI-TOF) *m/z*: [M+H]<sup>+</sup> Calcd for C<sub>24</sub>H<sub>21</sub>ClN<sub>3</sub>O<sub>2</sub>S 450.0964, Found 450.0966.

4.1.4.12. 5-(2,3-dihydrobenzo[b][1,4]dioxane-6-yl)-3-(3-methoxyphenyl)-N-phenyl-4,5-dihydro-1H-pyrazole-1-carbothioamide (**12**). Pale yellow solid; mp 136–138 °C; yield: 70%; <sup>1</sup>H NMR (600 MHz, DMSO-*d*<sub>6</sub>) δ 10.17 (s, 1H), 7.60 (s, 1H), 7.55 (d, *J* = 7.7 Hz, 2H), 7.51 (d, *J* = 7.7 Hz, 1H), 7.39 (t, *J* = 8.0 Hz, 1H), 7.35 (t, *J* = 7.7 Hz, 2H), 7.18 (t, *J* = 7.4 Hz, 1H), 7.08 (dd, *J* = 8.2, 2.4 Hz, 1H), 6.81 (d, *J* = 8.2 Hz, 1H), 6.67–6.65 (m, 2H), 5.94 (dd, *J* = 11.2, 3.1 Hz, 1H), 4.21 (s, 4H), 3.89 (dd, *J* = 18.1, 11.3 Hz, 1H), 3.83 (s, 3H), 3.21 (dd, *J* = 18.1, 3.3 Hz, 1H); <sup>13</sup>C NMR (151 MHz, DMSO) δ 174.22, 159.92, 155.89, 143.65, 142.86, 140.00, 136.26, 132.61, 130.28, 128.51, 126.16, 125.48, 120.53, 118.68, 117.63, 117.35, 114.46, 112.50, 64.56, 64.44, 63.27, 55.84, 42.55; HRMS (ESI-TOF) *m/z*: [M+H]<sup>+</sup> Calcd for C<sub>25</sub>H<sub>24</sub>N<sub>3</sub>O<sub>3</sub>S 446.1460, Found 446.1463.

4.1.4.13. 3-(3,4-dichlorophenyl)-5-(2,3-dihydrobenzo[b][1,4]dioxane-6-yl)-N-phenyl-4,5-dihydro-1H-pyrazole-1-carbothioamide (**13**). Yellow solid; mp 169–171 °C; yield: 78%; <sup>1</sup>H NMR (600 MHz, DMSO-*d*<sub>6</sub>) δ 10.30 (s, 1H), 8.37 (d, *J* = 2.0 Hz, 1H), 7.90 (dd, *J* = 8.4, 2.0 Hz, 1H), 7.75 (d, *J* = 8.4 Hz, 1H), 7.53 (d, *J* = 7.6 Hz, 2H), 7.36 (t, *J* = 7.6 Hz, 2H), 7.19 (t, *J* = 7.4 Hz, 1H), 6.81 (d, *J* = 8.1 Hz, 1H), 6.66–6.65 (m, 2H), 5.95 (dd, *J* = 11.3, 3.3 Hz, 1H), 4.21 (s, 4H), 3.88 (dd, *J* = 18.2, 11.5 Hz, 1H), 3.24 (dd, *J* = 18.2, 3.4 Hz, 1H); <sup>13</sup>C NMR (151 MHz, DMSO) δ 174.54, 154.91, 143.42, 142.62, 139.65, 136.52, 135.59, 128.45, 128.05, 126.06, 126.02, 125.88, 125.67, 125.18, 123.48, 118.50, 117.69, 114.49, 64.55, 64.43, 63.50, 42.30; HRMS (ESI-TOF) *m/z*: [M+H]<sup>+</sup> Calcd for C<sub>24</sub>H<sub>20</sub>Cl<sub>2</sub>N<sub>3</sub>O<sub>2</sub>S 484.0575, Found 484.0574.

4.1.4.14. 5-(2,3-dihydrobenzo[b][1,4]dioxane-6-yl)-3-(3,4-dimethylphenyl)-N-phenyl-4,5-dihydro-1H-pyrazole-1-carbothioamide (**14**). Pale yellow solid; mp 162–164 °C; yield: 72%; <sup>1</sup>H NMR (600 MHz, DMSO-*d*<sub>6</sub>) δ 10.09 (s, 1H), 7.79 (s, 1H), 7.69 (dd, *J* = 7.7, 1.4 Hz, 1H), 7.57 (d, *J* = 7.5 Hz, 2H), 7.34 (t, *J* = 7.6 Hz, 2H), 7.25 (d, *J* = 7.9 Hz, 1H), 7.16 (t, *J* = 7.4 Hz, 1H), 6.81 (d, *J* = 8.2 Hz, 1H), 6.66–6.64 (m, 2H), 5.93 (dd, *J* = 11.1, 3.0 Hz, 1H), 4.20 (s, 4H), 3.87 (dd, *J* = 17.9, 11.3 Hz, 1H), 3.17 (dd, *J* = 18.0, 3.2 Hz, 1H), 2.28 (s, 6H); <sup>13</sup>C NMR (151 MHz, DMSO) δ 174.56, 154.39, 143.67, 142.92, 139.91, 136.14, 135.32, 128.53, 128.51, 126.05, 126.00, 125.98, 125.54, 125.42, 123.62, 118.71, 117.65, 114.51, 64.55, 64.44, 63.59, 42.33, 40.52, 40.49; HRMS (ESI-TOF) *m/z*: [M+H]<sup>+</sup> Calcd for C<sub>26</sub>H<sub>26</sub>N<sub>3</sub>O<sub>2</sub>S 444.1667, Found 444.1665.

4.1.4.15. 3-(4-(benzyloxy)phenyl)-5-(2,3-dihydrobenzo[b][1,4]dioxane-6-yl)-N-phenyl-4,5-dihydro-1H-pyrazole-1-carbothioamide (**15**). Pale yellow solid; mp 203–205 °C; yield: 56%; <sup>1</sup>H NMR (600 MHz, DMSO-*d*<sub>6</sub>) δ 10.11 (s, 1H), 7.95 (d, *J* = 8.7 Hz, 2H), 7.61 (d, *J* = 8.0 Hz, 2H), 7.47 (d, *J* = 7.3 Hz, 2H), 7.40 (t, *J* = 7.4 Hz, 2H), 7.34 (t, *J* = 7.6 Hz, 3H), 7.16 (t, *J* = 7.4 Hz, 1H), 7.12 (d, *J* = 8.8 Hz, 2H), 6.82–6.81 (m, 1H), 6.68–6.67 (m, 2H), 5.94 (dd, *J* = 11.0, 2.5 Hz, 1H), 5.19 (s, 2H), 4.19 (s, 4H), 3.85 (dd, *J* = 17.9, 11.3 Hz, 1H), 3.16 (dd, *J* = 17.9, 2.9 Hz, 1H); <sup>13</sup>C NMR (151 MHz, DMSO) δ 173.92, 159.32, 157.00, 151.72, 148.73, 148.52, 138.55, 133.12, 129.56, 129.01, 128.99, 128.42, 128.40, 127.96, 127.41, 127.39, 126.52, 126.48, 121.80, 118.93, 118.60, 117.81, 117.62, 117.52, 111.98, 109.54, 64.56, 64.43, 63.42, 42.33; HRMS (ESI-TOF) *m/z*: [M+H]<sup>+</sup> Calcd for C<sub>30</sub>H<sub>28</sub>N<sub>3</sub>O<sub>3</sub>S 522.1851, Found 522.1847.

4.1.4.16. 5-(2,3-dihydrobenzo[b][1,4]dioxane-6-yl)-N-phenyl-3-(thiophen-2-yl)-4,5-dihydro-1H-pyrazole-1-carbothioamide (**16**). Pale yellow solid; mp 183–184 °C; yield: 76%; <sup>1</sup>H NMR (600 MHz, DMSO-*d*<sub>6</sub>) δ 9.92 (s, 1H), 7.82 (d, *J* = 4.9 Hz, 1H), 7.58–7.55 (m, 3H), 7.34–7.30 (m, 2H), 7.18 (dd, *J* = 4.9, 3.8 Hz, 1H), 7.15 (t, *J* = 7.4 Hz, 1H), 6.82 (d, *J* = 8.1 Hz, 1H), 6.68–6.66 (m, 2H), 5.98 (dd, *J* = 11.2, 3.0 Hz, 1H), 4.21 (s, 4H), 3.94 (dd, *J* = 17.8, 11.2 Hz, 1H), 3.19 (dd, *J* = 17.8, 3.1 Hz, 1H); <sup>13</sup>C NMR (151 MHz, DMSO) δ 174.12, 155.62, 148.74, 148.54, 135.50, 133.12, 129.01, 128.48, 128.42, 127.23, 126.99, 126.52, 125.24, 123.80, 125.62, 117.82, 115.93, 109.52, 65.23, 64.44, 62.20, 42.66; HRMS (ESI-TOF) *m/z*: [M+H]<sup>+</sup> Calcd for C<sub>22</sub>H<sub>20</sub>N<sub>3</sub>O<sub>2</sub>S<sub>2</sub> 438.0946, Found 438.0942.

## 4.2. Biological assay

### 4.2.1. Anti-proliferation assay

Human melanoma cells A375 (BRAF<sup>V600E</sup> mutated, ATCC CRL-1619), WM2664 (BRAF<sup>V600E</sup> mutated, from Nanjing University, P. R. China) and WM1361 (BRAF<sup>WT</sup>, from Nanjing University, P. R. China), human colon cancer cells HT29 (BRAF<sup>V600E</sup> mutated, ATCC HTB-38) and HCT116 (BRAF<sup>WT</sup>, ATCC CCL-247) together with human embryonic cells HEK293T (kidney, ATCC CRL-3216) and LO2 (liver, from Nanjing University, P. R. China) were used in this work. A375 was maintained in Dulbecco's modified Eagle's medium (DMEM) 12430 (Invitrogen) with Sodium Pyruvate (Invitrogen, 11360-070) added. The other cell lines grew in DMEM (Hyclone). All media was supplemented with 10% foetal bovine serum (FBS, BI), 2 mmol/L of L-glutamine, 100 units/mL of penicillin-streptomycin (Sigma-Aldrich), 100 mg/mL streptomycin (Hyclone) and incubated at 37 °C in a water saturated atmosphere containing 5% CO<sub>2</sub>.

The anti-proliferative activities of the prepared compounds against the cultured cells were evaluated using a standard MTT-based colorimetric assay with some modification. Cell lines grew to log phase in DMEM supplemented with 10% FBS (BI). Cell suspensions were prepared and 100 μL/well dispensed into 96-well plates to give 10<sup>4</sup> per well. The subsequent incubation was

performed at 37 °C, 5% CO<sub>2</sub> atmosphere for 24 h to allow reattaching. Subsequently, cells were treated with the target compounds at 0.001 μM, 0.01 μM, 0.1 μM, 1 μM, 10 μM, 100 μM and 500 μM in the presence of 10% FBS for 48 h. Afterwards, cell viability was assessed by the conventional 3-(4, 5-dimethylthiazol-2-yl)-2, 5-diphenyltetrazolium bromide (MTT) reduction assay carried out strictly according to the manufacturer's instructions (Sigma-Aldrich). The absorbance (OD<sub>570</sub>) was read on LX300 Epsilon Diagnostic micro-plate reader. Three replicate wells were used for each concentration and each assay was measured three times, after which the average of GI<sub>50</sub> was calculated. The GI<sub>50</sub> was calculated using SPSS 13.0 software.

### 4.2.2. Kinase inhibitory assay

This V600E mutant BRAF kinase assay was performed in triplicate for each tested compound in this study. Briefly, 7.5 ng Mouse Full-Length GST-tagged BRAF<sup>V600E</sup> (Invitrogen, PV3849) was pre-incubated at room temperature for 1 h with 1 μL drug and 4 μL assay dilution buffer. The kinase assay was initiated when 5 μL of a solution containing 200 ng recombinant human full length, N-terminal His-tagged MEK1 (Invitrogen, PV3093), 200 μM ATP, and 30 mM MgCl<sub>2</sub> in assay dilution buffer was added. The kinase reaction was allowed to continue at room temperature for 25 min and was then quenched with 5 μL 5 × protein denaturing buffer (LDS) solution. Protein was further denatured by heating for 5 min at 70 °C. 10 μL of each reaction was loaded into a 15-well, 4–12% precast NuPage gel (Invitrogen) and run at 200 V, and upon completion, the front, which contained excess hot ATP, was cut from the gel and discarded. The gel was then dried and developed onto a phosphor screen. A reaction that contained no active enzyme was used as a negative control, and a reaction without inhibitor was used as the positive control.

Detection of the effect of compounds on cell based pERK1/2 activity in WM2664 cells was performed using ELISA kits (Invitrogen) and strictly according to the manufacturer instructions.

The wild type BRAF kinase (Invitrogen, PV3848) and CRAF kinase (Invitrogen, PV3805) were evaluated use the same method as V600E mutant BRAF kinase.

Assays on p38α and JNK1 using radio labeled [γ-<sup>32</sup>P] ATP (HalingBio, Shanghai) were performed in 96 well plates. The p38α and JNK1 were expressed as N-terminal FLAG-tagged proteins using a baculovirus expression system. The reaction conditions were optimized for each kinase: p38α (100 ng per well of enzyme, 1 μg per well of MBP (Wako Pure Chemical Ind., Japan), 0.1 μCi per well of [γ-<sup>32</sup>P] ATP, 60 min reaction at 30 °C; JNK1 (10 ng per well of enzyme, 1 μg per well of c-Jun, 0.1 μCi per well of [γ-<sup>32</sup>P] ATP, 60 min reaction at 30 °C. The reactions were performed in 25 mM HEPES, pH 7.5, 10 mM magnesium acetate, 1 mM dithiothreitol and 0.5 μM ATP containing enzyme, substrate and radio labeled ATP as described above in a total volume of 50 μL. Prior to the kinase reaction, compound and enzyme were incubated for 5 min at reaction temperature as described above. The kinase reactions were initiated by adding ATP. After the reaction period as described above, the reactions were terminated by the addition of 10% (final concentration) trichloroacetic acid. The [γ-<sup>32</sup>P]-phosphorylated proteins were filtrated in Harvest Plate (STEMCELL Technologies Inc. Shanghai) with a Cell Harvester (PerkinElmer) and then free [γ-<sup>32</sup>P] ATP was washed out with 3% phosphoric acid. The plates were dried, followed by the addition of 40 μL of MicroScint0 (PerkinElmer). The radioactivity was counted by a Top Count scintillation counter (PerkinElmer).

### 4.2.3. Cell apoptosis and cell cycle analysis

Approximately 10<sup>5</sup> per well cells were cultured in a 24-well plate and allowed to adhere. Subsequently, the medium was

replaced with fresh culture medium containing compound **12** at final concentrations of 0, 2.5, 5, 10 and 20  $\mu\text{M}$ . Non-treated wells received an equivalent volume of ethanol (<0.1%). After 24 h, cells were trypsinized, washed in PBS and centrifuged at 2000 rpm for 5 min. The pellet was resuspended in 500  $\mu\text{L}$  staining solution (containing 5  $\mu\text{L}$  AnnexinV-FITC and 5  $\mu\text{L}$  PI (5 mg/mL) in Binding Buffer), mixed gently and incubated for 15 min at room temperature assay dilution buffer in dark. The samples were then analyzed by a FACSCalibur flow cytometer (Becton Dickinson, US). Time-dependent protocol was similar to the process above with concentration of **12** set as 2  $\mu\text{M}$  and incubation time varying (0, 24, 48 and 72 h).

Cells were plated in 6-well plates (10<sup>6</sup> per well) and incubated at 37 °C or 24 h. Exponentially growing cells were then incubated with compound **12** at different concentrations (0, 2.5, 5, 10 and 20  $\mu\text{M}$ ). After 24 h, cells were centrifuged at 1500 rpm at 4 °C for 5 min, fixed in 70% ethanol at 4 °C for at least 12 h and subsequently resuspended in phosphate buffered saline (PBS) containing 0.1 mg/mL RNase A and 5 mg/mL propidium iodide (PI). The cellular DNA content was measured by flow cytometry for cell cycle distribution analysis, plotting at least 10,000 events per sample. The percentage of cells in the subG0/G1, G0/G1, S and G2/M phases of the cell cycle were determined using Flowjo 7.6.1 software.

#### 4.2.4. Western blot

A375 cells on 6-well plates were rinsed twice with cold PBS and lysed in RIPA lysis buffer containing a protease inhibitor mixture at 1:100 dilution on ice for 30 min. The insoluble components of cell lysates were removed by centrifugation (4 °C, 12,000 g, 10 min). Protein concentrations were measured using a Pierce BCA protein assay kit. Proteins were separated by sodium dodecyl sulfate-polyacrylamide gel electrophoresis (SDS-PAGE) and transferred onto polyvinylidene difluoride (PVDF) membranes. Membranes were blocked using skim milk and then incubated with diluted indicated primary antibodies (1:500 dilution) at 4 °C with gentle shaking overnight. After washing five times, membranes were incubated with secondary antibody (1:5000 dilution) for 1 h at room temperature.

#### 4.2.5. Xenograft model

Cultured A375 cells were washed and resuspended in cold PBS. Portions of the suspension (3  $\times$  10<sup>6</sup> cells in 0.1 mL) were injected into the right flank of nude mice. The treatment was initiated when tumor volume reached approximately 100 mm<sup>3</sup> and mice were randomized into groups (5 mice in each group). Compound **12** and positive control vemurafenib were suspended at the desired concentration as needed for each dose group in olive oil. Then they were administered every second day for 14 days by intraperitoneal injection. Body weight were monitored and recorded every two days. Tumor tissues were excised and weighted on day 15. Animal welfare and experimental procedures were followed in accordance with the Guide for Care and Use of Laboratory Animals (National Institutes of Health, the United States) and the related ethical regulations of Nanjing University.

#### 4.3. Experimental protocol of ADMET study

The three-dimensional structures of the aforementioned compounds were constructed using Chem. 3D ultra 14.0 software [Chemical Structure Drawing Standard; Cambridge Soft corporation, USA (2015)]. Then they were minimized a CHARMM based force field the same as in docking study. The ADMET study was conducted using the Calculate Molecular Properties in Small Molecules module of the Discovery Studio (version 3.5). The ADMET properties map and data were provided by the ADMET Descriptors

tool.

#### 4.4. Experimental protocol of docking study

The three-dimensional structures of the aforementioned compounds were constructed using Chem. 3D ultra 14.0 software [Chemical Structure Drawing Standard; Cambridge Soft corporation, USA (2015)]. The crystal structures of BRAF<sup>V600E</sup> (PDB Code: 1UWJ) and BRAF<sup>WT</sup> (PDB Code: 1UWH) were retrieved from the RCSB Protein Data Bank (<http://www.rcsb.org>). All bound waters and ligands were eliminated from the protein and the polar hydrogen was added to the proteins. Molecular docking of all compounds including preliminary designed ones was then carried out using the Discovery Studio (version 3.5) as implemented through the graphical user interface CDOCKER protocol.

CDOCKER is an implementation of a CHARMM based molecular docking tool using a half-flexible receptor, including the following steps:

- (1) A series of ligands conformations are generated using high temperature molecular dynamics with different random seeds.
- (2) Random orientations of the conformations are generated by translating the center of the ligand to a specified position within the receptor active site, and making a series of random rotations. A softened energy is calculated and the orientation is kept when it is less than a specified limit. This process repeats until either the desired number of low-energy orientations is obtained, or the test times of bad orientations reached the maximum number.
- (3) Each orientation is subjected to simulated annealing molecular dynamics. The temperature is heated up to a high temperature then cooled to the target temperature. A final energy minimization of the ligand in the rigid receptor using non-softened potential is performed.
- (4) For each of the final pose, the CHARMM energy (interaction energy plus ligand strain) and the interaction energy alone are figured out. The poses are sorted according to CHARMM energy and the top scoring (most negative, thus favorable to binding) poses are retained. The whole kinase domain defined as a receptor and the site sphere was selected based on the original ligand binding location, then the original ligand was removed and the ligands prepared by us were placed during the molecular docking procedure. CHARMM was selected as the force field. The molecular docking was performed with a simulated annealing method. The heating steps were 2000 with 700 of heating target temperature. The cooling steps were 5000 with 300 cooling target temperature. Ten molecular docking poses saved for each ligand were ranked according to their dock score function. The pose with the highest -CDOCKER energy was chosen as the most suitable pose.

#### Ethical statement

Animal welfare and experimental procedures were followed in accordance with the Guide for Care and Use of Laboratory Animals (National Institutes of Health, the United States) and the related ethical regulations of Nanjing University.

#### Acknowledgment

This work is supported by the Public Science and Technology Research Funds Projects of Ocean (No. 201505023), the Fundamental Research Funds for the Central Universities (No.

020814380063) and Jiangsu Planned Projects for Postdoctoral Research Funds (No. 1701091C).

## Appendix A. Supplementary data

Supplementary data related to this article can be found at <https://doi.org/10.1016/j.ejmech.2018.06.043>.

## References

- [1] J. Ferlay, I. Seorjomataram, R. Dikshit, S. Eser, C. Mathers, M. Rebelo, D.M. Parkin, D. Forman, F. Bray, Cancer incidence and mortality worldwide: sources, methods and major patterns in GLOBOCAN 2012, *Int. J. Canc.* 136 (2015) E359–E386.
- [2] C. Wellbrock, M. Karasarides, R. Marais, The RAF proteins take centre stage, *Nat. Rev. Mol. Cell Biol.* 5 (2004) 875–885.
- [3] P. Marchetti, A. Trinh, R. Khamari, J. Kluza, Melanoma metabolism contributes to the cellular responses to MAPK/ERK pathway inhibitors, *BBA-Gen. Subjects* 1862 (2018) 999–1005.
- [4] H. Davies, G.R. Bignell, C. Cox, P. Stephens, S. Edkins, et al., Mutations of the BRAF gene in human cancer, *Nature* 417 (2002) 949–954.
- [5] N. Li, D. Batt, M. Warmuth, B-Raf kinase inhibitors for cancer treatment, *Curr. Opin. Invest. Drugs* 8 (2007) 452–456.
- [6] G. Maurer, B. Tarkowski, M. Baccarini, Raf kinases in cancer-roles and therapeutic opportunities, *Oncogene* 30 (2011) 3477–3488.
- [7] M. Burotto, V.L. Chiou, J.M. Lee, E.C. Kohn, The MAPK pathway across different malignancies: a new perspective, *Cancer* 120 (2014) 3446–3456.
- [8] B. Rodenak-Kladniew, A. Castro, P. Starkel, C. De Saeger, M.G. De Bravo, R. Crespo, Linalool induces cell cycle arrest and apoptosis in HepG2 cells through oxidative stress generation and modulation of Ras/MAPK and Akt/mTOR pathways, *Life Sci.* 199 (2018) 48–59.
- [9] S.J. Heidorn, Combined BRAF and MEK inhibition versus BRAF inhibition alone in melanoma, *N. Engl. J. Med.* 371 (2014) 1877–1888.
- [10] Y. Cohen, M. Xing, E. Mambo, Z. Guo, G. Wu, B. Trink, U. Beller, W.H. Westra, P.W. Ladenson, D. Sidransky, BRAF mutation in papillary thyroid carcinoma, *J. Natl. Cancer Inst.* 95 (2004) 625–627.
- [11] M. Xing, BRAF mutation in papillary thyroid cancer: pathogenic role, molecular bases, and clinical implications, *Endocr. Rev.* 28 (2016) 742–762.
- [12] X. Xu, R.M. Quiros, P. Gattuso, K.B. Ain, R.A. Prinz, High prevalence of BRAF gene mutation in papillary thyroid carcinomas and thyroid tumor cell lines, *Canc. Res.* 63 (2003) 4561–4567.
- [13] G. Singer, R. Oldt, Y. Cohen, B.G. Wang, D. Sidransky, R.J. Kurman, I.M. Shih, Mutations in BRAF and KRAS characterize the development of low-grade ovarian serous carcinoma, *J. Natl. Cancer Inst.* 95 (2003) 484–486.
- [14] K.T. Kuo, T.L. Mao, S. Jones, E. Veras, A. Ayhan, T.L. Wang, R. Glas, D. Slamon, V.E. Velculescu, R.J. Kuman, I.M. Shih, Frequent activating mutations of PIK3CA in ovarian clear cell carcinoma, *Am. J. Pathol.* 174 (2009) 1597–1601.
- [15] H.R. Harris, M.S. Rice, A.L. Shafir, E.M. Poole, M. Gupta, J.L. Hecht, K.L. Terry, S.S. Tworoger, Lifestyle and reproductive factors and ovarian cancer risk by p53 and MAPK expression, *Cancer Epidemiol. Biomarkers* 27 (2018) 96–102.
- [16] L. Si, X.S. Zhang, Z. Xu, Q.D. Jiang, L.L. Bu, X. Wang, L.L. Mao, W.J. Zhang, N. Richie, J. Guo, Vemurafenib in Chinese patients with BRAF<sup>V600</sup> mutation-positive unresectable or metastatic melanoma: an open-label, multicenter phase I study, *BMC Canc.* 18 (2018), 520.
- [17] J.J. Grob, Is there any interest in a new BRAF-MEK inhibitor combination in melanoma? *Lancet Oncol.* 19 (2018) 580–581.
- [18] K. Kalinsky, F.G. Haluska, Novel inhibitors in the treatment of metastatic melanoma, *Expert Rev. Anticancer Ther.* 7 (2007) 715–724.
- [19] A.S. Dhillon, S. Hagan, O. Rath, W. Kolch, MAP kinase signalling pathways in cancer, *Oncogene* 26 (2007) 3279–3290.
- [20] P.T. Wan, M.J. Garnett, S.M. Roe, S. Lee, D. Niculescu-Duvaz, V.M. Good, C.M. Jones, C.J. Marshall, C.J. Springer, D. Barford, R. Marais, C.G. Project, Mechanism of activation of the RAF-ERK signaling pathway by oncogenic mutations of B-RAF, *Cell* 116 (2004) 855–867.
- [21] A.P. Algazi, E. Cha, S.M. Ortiz-Urda, T. McCalmont, B.C. Bastian, J. Hwang, M.H. Pampaloni, S. Behr, K. Chong, B. Cortez, A. Quiroz, F. Coakley, S. Liu, A.I. Daud, The combination of axitinib followed by paclitaxel/carboplatin yields extended survival in advanced BRAF wild-type melanoma: results of a clinical/correlative prospective phase II clinical trial, *Br. J. Canc.* 112 (2015) 1326–1331.
- [22] K. Kurata, N. Onoda, S. Noda, S. Kashiwagi, Y. Asano, K. Hirakawa, M. Ohira, Growth arrest by activated BRAF and MEK inhibition in human anaplastic thyroid cancer cells, *Int. J. Oncol.* 49 (2016) 2303–2308.
- [23] Z.Y. Abd Elmageed, R.F. Moore, K. Tsumagari, M.M. Lee, A.B. Sholl, P. Friedlander, Z. Al-Qurayshi, M. Hassan, A.R. Wang, H.A. Boulares, E. Kandil, Prognostic Role of BRAF<sup>V600E</sup> Cellular Localization in Melanoma, vol 226, 2017, pp. 526–537.
- [24] J. Chesney, Y. Imbert-Fernandez, S. Telang, M. Baum, S. Ranjan, M. Fraig, N. Batty, Potential clinical and immunotherapeutic utility of talimogene laherparepvec for patients with melanoma after disease progression on immune checkpoint inhibitors and BRAF inhibitors, *Melanoma Res.* 28 (2018) 250–255.
- [25] Y. Cui, T.M. Guadagno, B-Raf(V600E) signaling deregulates the mitotic spindle checkpoint through stabilizing Mps1 levels in melanoma cells, *Oncogene* 27 (2008) 3122–3133.
- [26] P. Koelblinger, O. Thuerigen, R. Dummer, Development of encorafenib for BRAF-mutated advanced melanoma, *Curr. Opin. Oncol.* 30 (2018) 125–133.
- [27] B. Agianian, E. Gavathiotis, Current insights of BRAF inhibitors in Cancer, *J. Med. Chem.* <https://doi.org/10.1021/acs.jmedchem.7b01306>.
- [28] S. Mathieu, S.N. Gradl, L. Ren, Z. Wen, I. Aliagas, et al., Potent and selective aminopyrimidine-based B-Raf inhibitors with favorable physicochemical and pharmacokinetic properties, *J. Med. Chem.* 55 (2012) 2869–2881.
- [29] A.J. King, D.R. Patrick, R.S. Batorsky, M.L. Ho, H.T. Do, et al., Demonstration of a genetic therapeutic index for tumors expressing oncogenic BRAF by the kinase inhibitor SB-590885, *Canc. Res.* 66 (2006) 11100–11105.
- [30] C. Blackburn, M.O. Duffey, A.E. Gould, B. Kulkarni, J.X. Liu, S. Menon, M. Nagayoshi, T.J. Vos, J. Williams, Discovery and optimization of N-acyl and N-aroylpyrazolines as B-Raf kinase inhibitors, *Bioorg. Med. Chem. Lett* 20 (2010) 4795–4799.
- [31] C.Y. Li, Q.S. Li, L. Yan, X.G. Sun, R. Wei, H.B. Gong, H.L. Zhu, Synthesis, biological evaluation and 3D-QSAR studies of novel 4,5-dihydro-1H-pyrazole niacinamide derivatives as BRAF inhibitors, *Bioorg. Med. Chem.* 20 (2012) 3746–3755.
- [32] Y.S. Yang, Q.S. Li, S. Sun, Y.B. Zhang, X.L. Wang, F. Zhang, J.F. Tang, H.L. Zhu, Design, modification and 3D QSAR studies of novel 2,3-dihydrobenzo[b][1,4]dioxin-containing 4,5-dihydro-1H-pyrazole derivatives as inhibitors of B-Raf kinase, *Bioorg. Med. Chem.* 20 (2012) 6048–6058.
- [33] Y.S. Yang, B. Yang, Y. Zou, G. Li, H.L. Zhu, Design, Biological Evaluation and 3D QSAR Studies of Novel Dioxin-containing Triaryl Pyrazoline Derivatives as Potential B-Raf Inhibitors, vol 24, 2016, pp. 3052–3061.
- [34] H. Khalilullah, S. Khan, M.J. Ahsan, B. Ahmed, Synthesis and antihepatotoxic activity of 5-(2,3-dihydro-1,4-benzodioxane-6-yl)-3-substituted-phenyl-4,5-dihydro-1H-pyrazole derivatives, *Bioorg. Med. Chem. Lett* 21 (2011) 7251–7254.
- [35] H.H. Wang, K.M. Qiu, H.E. Cui, Y.S. Yang, Y. Luo, M. Xing, X.Y. Qiu, L.F. Bai, H.L. Zhu, Synthesis, molecular docking and evaluation of thiazolyl-pyrazoline derivatives containing benzodioxole as potential anticancer agents, *Bioorg. Med. Chem.* 21 (2013) 448–455.